Risks of hypoxia and acidification in the high energy coastal environment near Victoria, Canada's untreated municipal sewage outfalls

Jeremy Krogh, Debby Ianson, Roberta C. Hamme, Christopher J. Lowe

2018

Marine Pollution Bulletin 133 (2018) 517–531

Contents lists available at ScienceDirect

Marine Pollution Bulletin

journal homepage: www.elsevier.com/locate/marpolbul

Risks of hypoxia and acidification in the high energy coastal environment near Victoria, Canada's untreated municipal sewage outfalls

Jeremy Krogh[a,c,*], Debby Ianson[a,b], Roberta C. Hamme[a], Christopher J. Lowe[c]

[a] School of Earth and Ocean Sciences, University of Victoria, Victoria, British Columbia, Canada
[b] Fisheries and Oceans Canada, Institute of Ocean Sciences, Sidney, British Columbia, Canada
[c] Capital Regional District, Victoria, British Columbia, Canada

ARTICLE INFO

Keywords:
Hypoxia
Sewage outfall
Ocean acidification
Dissolved oxygen
Victoria BC

ABSTRACT

Wastewater disposal often has deleterious impacts on the receiving environment. Low dissolved oxygen levels are particularly concerning. Here, we investigate the impacts on dissolved oxygen and carbon chemistry of screened municipal wastewater in the marine waters off Victoria, Canada. We analyzed data from undersea moorings, ship-based monitoring, and remotely-operated vehicle video. We used these observations to construct a two-layer model of the nearfield receiving environment. Despite the lack of advanced treatment, dissolved oxygen levels near the outfalls were well above a 62 μmol kg^{-1} hypoxic threshold. Furthermore, the impact on water column oxygen at the outfall is likely < 2 μmol kg^{-1}. Dissolved inorganic carbon is not elevated and pH not depressed compared to the surrounding region. Strong tidal currents and cold, well-ventilated waters give Victoria's marine environment a high assimilative capacity for organic waste. However, declining oxygen levels offshore put water near the outfall at risk of future hypoxia.

1. Introduction

The occurrence of hypoxia in coastal zones and its accompanying negative impacts on marine ecosystems has increased in recent decades (Gilbert et al., 2010; Diaz and Rosenberg, 2008; Diaz and Rosenburg, 1995). In many cases, anthropogenic inputs of nutrients from farm-runoff, wastewater, and atmospheric deposition are responsible (Rabalais et al., 2010). In attempts to mitigate the impacts from wastewater, environmental managers in many developed countries have implemented minimum treatment standards to reduce organic enrichment (Law and Tang, 2016; Canadian Fisheries Act; Igbinosa and Okoh, 2009).

In addition to treatment, the properties of the receiving environment are critical in determining the ultimate impacts of the waste (Puente and Diaz, 2015; Gómez et al., 2014; Dinn et al., 2012a; Li and Hodgins, 2010; Chapman et al., 1996). For example, if waste is discharged close to bathing waters or in a constrained environment, the public health risks are considerable. Or, if discharged into a nutrient-limited environment, as is often the case for freshwater (e.g. Lake Winnipeg, Schindler et al., 2012) or sheltered marine ecosystems (e.g. the Baltic Sea, Ronnberg and Bonsdorff, 2004), eutrophication can result. The frequency of harmful or otherwise undesirable algal blooms can increase and the rapid growth of aquatic plants can poison wildlife, contaminate drinking water, and deplete oxygen to hypoxic levels (Smith and Schindler, 2009; Tchobanoglous and Burton, 1991). However, if discharges enter non-nutrient-limited or high turnover environments, impacts on oxygen are generally smaller. However, the organic load within the sewage itself can be considerable, and, if the respiration of sewage organic material occurs in a small area, significant oxygen depletion and hypoxia can occur. As with all respiration, inorganic carbon is released, lowering the pH of water and increasing ocean acidification in the local marine environment (Cai et al., 2011). Low oxygen combined with lower pH and warmer water temperatures have the potential to act synergistically to the detriment of many marine organisms (Haigh et al., 2015). Chemical contamination of the receiving environment with metals and persistent organic pollutants is of universal concern (Balasubramani et al., 2014; Chapman, 2007; Tchobanoglous and Burton, 1991). However, these contaminant concerns are often secondary to the eutrophic and oxygen-depleting impacts of domestic sewage (Tchobanoglous and Burton, 1991).

In this study, we investigate the impact of untreated sewage on a unique, highly energetic, well-ventilated, marine receiving environment. We use temporally resolved multi-year time series of near bottom O_2 and ship-based vertical profiles at the outfall to quantify the impact on water column oxygen by sewage. These results are supplemented by spectral analyses of ambient oxygen and sewage volume flow and

* Corresponding author at: School of Earth and Ocean Sciences, University of Victoria, Victoria, British Columbia V8W 2Y2, Canada.
E-mail addresses: jkrogh@uvic.ca (J. Krogh), debby.ianson@dfo-mpo.gc.ca (D. Ianson), rhamme@uvic.ca (R.C. Hamme), clowe@crd.bc.ca (C.J. Lowe).

https://doi.org/10.1016/j.marpolbul.2018.05.018
Received 21 August 2017; Received in revised form 4 May 2018; Accepted 10 May 2018
Available online 19 June 2018
0025-326X/

qualitative analysis of benthic species composition. Discrete sampling of the carbonate system at the outfall is used to investigate potential acidification. Water masses are characterized and the tidal control of O_2 variability at the site is assessed, allowing risk assessment for future hypoxia. Finally, a simple two-box model is constructed to assess the sewage impact on the region at present-day and under future conditions of increased sewage volume and temperature.

2. Study site and regional oceanography

Greater Victoria, the capital city of British Columbia (BC), Canada, (Fig. 1a) is a lightly industrialized city home to nearly 350,000 inhabitants (Statistics Canada, 2012). The greater Victoria region has come under increasing public and international pressure to upgrade its sewage treatment system, which currently consists of only pre-treatment (6 mm screen) before discharge into the ocean in Juan de Fuca Strait, JdF (CRD, 2014).

This discharge is split between two major sewage outfalls located at Clover and Macaulay Points (Fig. 1b). The pipes extend 1.1 and 1.8 km offshore, respectively, to depths of 62 m and 67 m, making them relatively deep and far from shore (Philip and Pritchard, 1997). At the end of each outfall, wastewater is discharged through a series of small diffuser ports along the final 150 m of the outfall pipe (Fig. 1b inset) designed to maximize mixing and dilution. Both outfalls experience strong tidal currents (~1 m s^{-1}), with Clover experiencing slightly stronger currents (Chandler, 1997). The dominant bottom current direction, as determined by mooring studies, is to the southeast, matching a general pattern of seafloor sediment contamination (Krogh et al., 2017; Dinn et al., 2012b; Chandler, 1997; CRD, 2014; Chapman et al., 1996). Water temperatures are consistently cool, varying seasonally between 7 °C in the winter and 10 °C in the summer (Chandler, 1997). Thus, compared with many other coastal cities, Victoria is blessed with highly

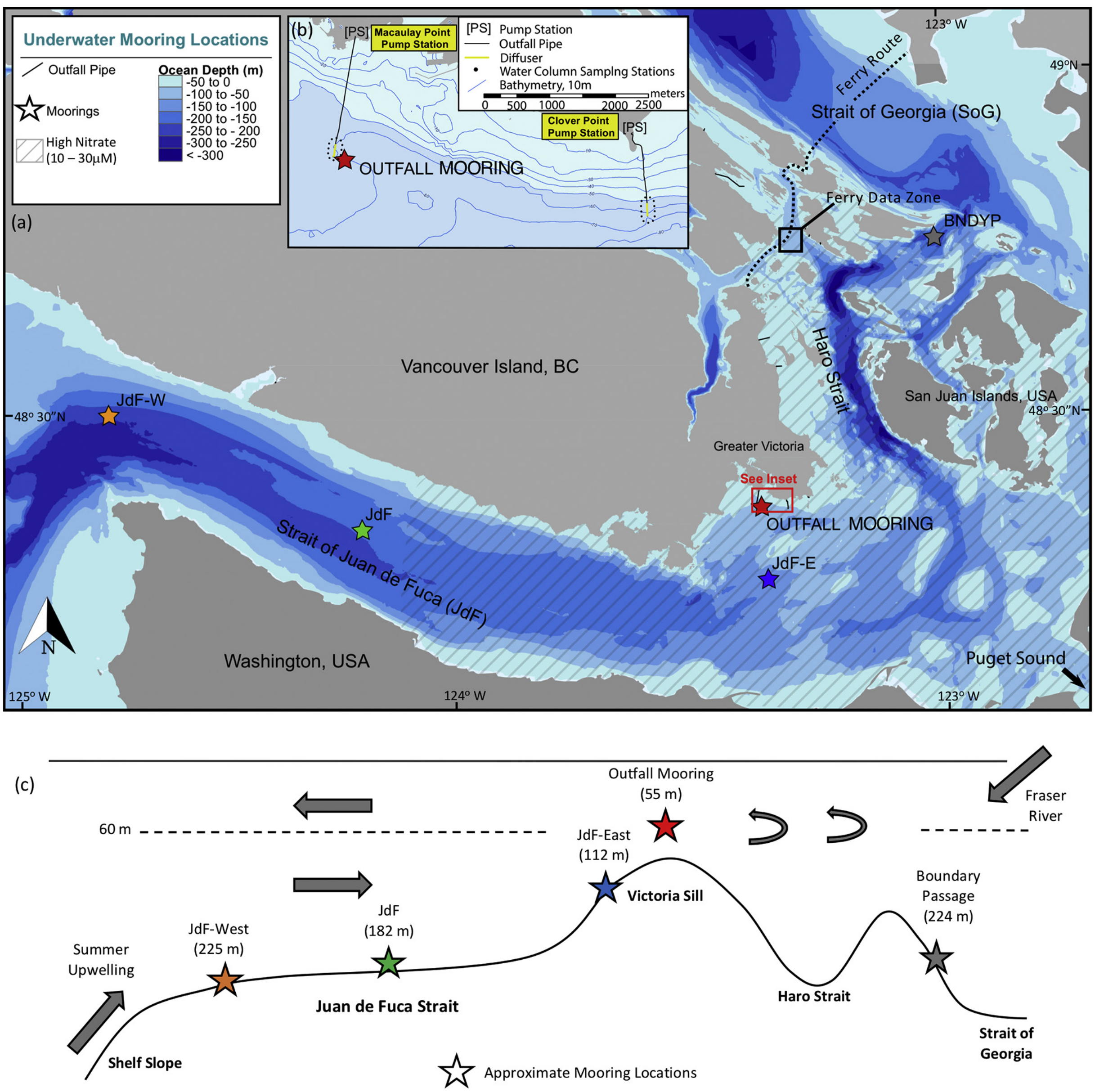

Fig. 1. (a) Map of the region, the colored stars show the locations of sea bottom moorings, the hashed area is a zone of high surface nutrients where primary production is light limited year-round (Mackas and Harrison, 1997). (b) Close-up map of the sewage outfalls with the black dots showing the location of monitoring stations where DIC/TA samples were collected and vertical profiles taken. (c) Schematic cross-section of the average flow and approximate depth along the thalweg. The outfall mooring is not located along the thalweg, but is still attached to the seabed, north of the thalweg nearer to shore. While there are two outfalls, Clover Point and Macaulay Point, only the less energetic Macaulay Point was monitored with a mooring.

favourable oceanographic conditions for the assimilation of organic waste.

The seabed around the more energetic Clover Point outfall is rocky and sedimentation is minimal (Diaz, 1992; CRD, 2014; Markovic, 2003). Around the Macaulay outfall, the seabed is made up of a mixture of sediment size classes (Diaz, 1992; Dinn et al., 2012a; Krepakevich and Pospelova, 2010; Markovic, 2003) ranging from fines to gravel. The area around the Macaulay outfall is also littered with garbage from when the area served as greater Victoria's municipal garbage dump between 1908 and 1958 (Ringuette, 2009). Some of this garbage (mainly glass, ceramics, and leather) is now buried a few centimeters below the surface (Shirley Lyons, Scientific Officer CRD, personal communication), indicating at least patchy sedimentation in the area (Krogh, 2017).

The JdF is a long (150 km), deep (250 m), and wide (25 km) channel containing the maritime boundary between Canada and the USA and connects the Pacific Ocean to the catchment basins of the Strait of Georgia (SoG) to the North-East and Puget Sound to the South (Fig. 1a). These three main basins form an area known as the Salish Sea. The innermost basins, SoG and Puget Sound, receive large volumes of freshwater runoff (LeBlond, 1983), and together the three basins form an estuarine complex, with JdF acting as an outer estuary (Thomson et al., 2007).

The largest source of fresh water enters the complex via the SoG from the snow-melt-fed Fraser River (1000–9000 $m^3 s^{-1}$), whose flow peaks in early summer (May–June) and reaches its annual minimum in late winter, with a secondary peak occasionally occurring in late fall due to heavy rains (Morrison et al., 2002). Puget Sound, meanwhile, receives approximately 2200 $m^3 s^{-1}$ of runoff, with no strong seasonal cycle (Thomson et al., 2007). Estuarine circulation is strong throughout the year in the JdF. The mean transition depth between the surface seaward and sub-surface landward flows is 60 m (Thomson et al., 2007), nearly the exact same depth as Victoria's sewage outfalls.

Along the western shelf off Vancouver Island, summer winds bring upwelling (Crawford and Thomson, 1991) and allow hypoxic, nutrient-, and carbon-rich shelf-slope waters (Ianson et al., 2003; Crawford and Peña, 2016) to enter the landward-flowing bottom layer of JdF (Davenne et al., 2001). The shelf-slope water moves south-east along the bottom of JdF as far as Victoria before being significantly altered by mixing with surface layers originating in the SoG (Pawlowicz, 2001). In winter, downwelling winds predominate along the outer coast, and oxygen concentrations rebound in the bottom layers of JdF as recently ventilated water flows into the deep JdF (Davenne et al., 2001).

Important to the region's oxygen dynamics is Haro Strait (Fig. 1) that connects JdF with SoG. Haro Strait is a complex of shallow sills and narrow channels that, combined with large tidal ranges of up to 4 m, induce intense mixing and allow JdF to operate as a separate estuarine circulation cell (Fig. 1). Surface waters enter Haro Strait's north-eastern end from the SoG, while deep waters from JdF enter Haro Strait's southern end. Strong tidal mixing of these water masses injects nutrients from deep JdF water into the surface layers of Haro Strait; much of this nutrient rich water subsequently flows into the surface layers of JdF, creating a large zone where primary production is limited by light not nutrients (hashed area Fig. 1a, Mackas and Harrison, 1997). At the same time, the vigorous mixing allows large amounts of oxygen from the atmosphere to diffuse into the water and be mixed throughout the water column (Ianson et al., 2016). Mixing is so complete that stratification breaks down, forcing the majority of water entering Haro Strait from JdF to be mixed into the surface and exit Haro Strait in the outward-flowing surface layer. Thus, much of the JdF landward flowing bottom water that enters Haro Strait never reaches the SoG (Pawlowicz et al., 2007).

Oceanographic zones with such consistent and high levels of vertical mixing are relatively rare and even less common adjacent to urban centres. For example, although parts of the North Channel neighbouring Belfast (Ireland) also experience intense mixing and limited water column stratification, light is not always limiting to phytoplankton growth and local nutrient concentrations appear to be anthropogenically enhanced (Parker et al., 1988). Thus, greater Victoria faces unique and reduced challenges with respect to liquid waste disposal.

3. Methods

3.1. Observational

3.1.1. Vertical profiles

Ship-based (*MSV John Strickland*) monitoring near the outfalls was carried out on five days each season between fall 2011 and fall 2016. Stations were located approximately 100 m from the sewage diffusers (black dots, Fig. 1b). On each sampling day, four stations were sampled based on the conditions at the time in order to maximize the chance of plume detection (i.e. in the down current direction as predicted by an oceanographic model; Hodgins, 2006). Vertical profiles were measured with a Seabird SBE-19 plus V2 conductivity, temperature, and pressure (CTD) sensor ($\pm$ 0.0007 on the PSS-78 scale, $\pm$ 0.005 °C, $\pm$ 0.1%) equipped with an SBE-43 oxygen sensor ($\pm$ 2% of saturation). Niskin bottles attached to a rosette were used to collect water samples for various analyses (including fecal coliform; CRD, 2014; Krogh, 2017) from three depths (roughly surface ~5 m, mid-depth ~40–50 m, and ~5 m above the bottom).

Inorganic carbon and total alkalinity

On four occasions (22 Jul 2015, 9 Nov 2015, 26 Jul 2016, and 24 Jan 2017), discrete dissolved inorganic carbon (DIC, $\pm$ 2 $\mu mol\ kg^{-1}$) and total alkalinity (TA, $\pm$ 4 $\mu mol\ kg^{-1}$) samples were collected from Niskin bottles on select profiles (Fig. 1b) and were analyzed according to Dickson et al. (2007). Aragonite saturation and pH were calculated using the MATLAB® version of CO2SYS (van Heuven et al., 2011). Nutrient concentrations (phosphate and silicic acid) required for these calculations were estimated from their relationship with salinity in the region (Krogh, 2017), with the exception of 24 Jan 2017 for which discrete nutrient data (analyzed following Barwell-Clark and Whitney, 1996) were collected along with DIC and TA.

3.1.2. Mooring network

In February 2013, a bottom-mounted mooring (instruments approximately 6 m off the seabed) was placed approximately 200 m downstream (southeast) of the less energetic (Chandler, 1997) Macaulay Point sewage outfall (Fig. 1). The mooring was equipped with a Sea-Bird SBE-37SMP CTD ($\pm$ 0.0006 PSS-78, $\pm$ 0.002 °C, $\pm$ 0.1%), SBE-63 oxygen (O_2) optode (greater of $\pm$ 3 $\mu mol\ kg^{-1}$ or $\pm$ 2%), and a Nortek Aquadopp acoustic current meter ($\pm$ 1 $cm\ s^{-1}$, $\pm$ 2°). This mooring is identical to four others placed in the region (Ocean Networks Canada, ONC, www.oceannetworks.ca) in 2012 (Fig. 1a). Individual mooring deployments lasted 4–12 months (Krogh, 2017). Combined, these deployments make up a four-and-a-half-year time series spanning November 2012 to October 2016. Data from the various deployments were merged together and binned to 1-hour intervals. Linear corrections were applied to correct O_2 sensor drift (~1% yr^{-1}) as quantified by routine manufacturer calibrations (Krogh, 2017). Sensor drift of the temperature (T) and salinity (S) sensors was below detection, and no correction was applied.

Time series analysis

Because sub-surface O_2 concentrations in the region are lowest during the summer upwelling season, we focused our analysis on summer. We defined summer based on the timing of upwelling near the western entrance of JdF, which typically spans year-day 138–225 (Bylhouwer et al., 2013). Hourly mooring data (T, S, O_2) were filtered with a 25-hour running mean to remove tidal effects (Section 4.1.2). In addition, power spectral analysis (Welch, 1967) was carried out on the data from the mooring and on the time series of sewage discharge over the same time period (Krogh, 2017).

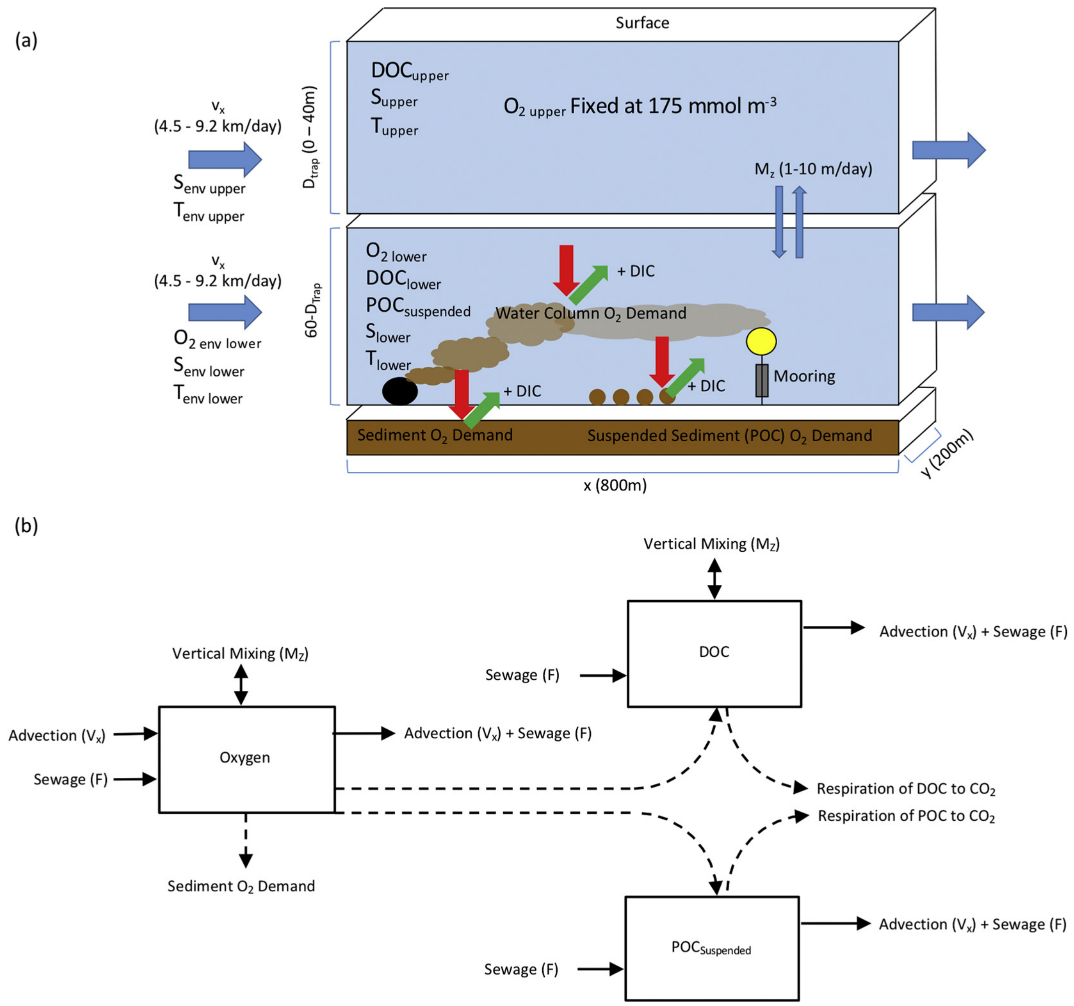

Fig. 2. (a) Cartoon of the sewage plume and processes affecting T, S, O_2, and DIC near the outfall within the physical structure of the mass balance model. Red arrows show oxygen consumption and green arrows show DIC production. Modelled quantities are listed at the left side of each box and in Table 1a. In the model, these quantities are perfectly mixed within their respective layers. Daily averaged net ocean currents are indicated for the long direction, cross direction currents are not shown but range from 0.9–3.5 km day^{-1} (25th and 75th percentiles). (b) Flow of O_2 shown schematically as physical and biological (i.e. consumption by organic matter) modelled fluxes in the lower layer of the model. Solid arrows represent volume fluxes that affect the O_2 concentration while dotted arrows represent biological fluxes (consumption). T and S (not shown) only experience physical fluxes, i.e.; advection, vertical mixing and dilution by sewage.

Table 1a
Modelled quantities.

Name	Simulated	Prescribed	Units
Dissolved oxygen	$O_{2\ lower}$	$O_{2\ env\ lower}$, $O_{2\ sewage}$, $O_{2\ upper}$	mmol m^{-3}
Salinity	S_{upper}, S_{lower}	$S_{env\ upper}$, $S_{env\ lower}$, S_{sewage}	kg m^{-3}
Temperature	T_{upper}, T_{lower}	$T_{env\ upper}$, $T_{env\ lower}$, T_{sewage}	°C
Organic carbon (dissolved sewage)	DOC_{upper}, DOC_{lower}	–	mmol m^{-3}
Organic carbon particles (sewage particles)	$POC_{suspended}$	–	mmol m^{-3}

3.1.3. *Ferry box underway system*

In addition to the mooring data set, we used surface measurements collected by an underway system aboard the BC Ferries vessel *Spirit of Vancouver Island*. The system collected data as the ferry crosses the north end of Haro Strait (Fig. 1a). T and S were measured with a Sea-Bird SBE 21 SeaCAT Thermosalinograph (± 0.01 °C, ± 0.005 PSS-78) and O_2 with an Anderaa optode 3835 (greater of ± 5 µM or 5%) (www.oceannetworks.ca).

3.2. *Model methods*

To further assess and quantify the impact of present day and future sewage on O_2 and DIC near the outfall, we created a two-box model. The model simulates S, T, and sewage-derived dissolved organic carbon (DOC) in both the upper and lower boxes (Fig. 2, Table 1a). In addition, O_2 and sewage-derived particulate organic carbon (POC) are simulated in the lower box. We determine a predicted O_2 deficit by comparing each model run to a parallel simulation with identical input parameters but without sewage. Model parameters (Appendix Tables A.1 & A.2) were fixed for each model run but were varied one at a time between runs (within the ranges stated) to assess the model's sensitivity. The model was run to steady state numerically using a Runge-Kutta solver with a dynamic time step (Shampine and Reichelt, 1997; Krogh, 2017). Mixing within each box was assumed to occur instantly so that all model quantities were homogenized.

3.2.1. Physical model

The water column (60 m in total) was divided into an upper and a lower box. The division between the upper and lower boxes is the trapping depth (D_{Trap}), defined as the depth above which the majority of sewage does not rise. D_{Trap} is shallower than the estuary circulation transition depth of ~60 m between landward and seaward flowing layers in JdF (Thomson et al., 2007). Bacteriological observations (Section 3.1.1) show that the sewage plume is normally trapped below 40 m depth (D_{Trap} = 40 m) (CRD, 2014), but at times can be confined below 50 m (D_{Trap} = 50 m) or, rarely (< 2% of observations), can rise to the surface (D_{Trap} = 0 m) (CRD, 2014; Lorax, 2009).

Near-surface (5 m) fecal bacteria concentrations were compared with those observed within the sewage to calculate the amount of sewage dilution and, thus, the vertical transport of sewage (i.e. vertical mixing) into the upper box. Although fecal bacteria is a non-conservative tracer of sewage (die-off rates can exceed 90% in 12 h (Lorax, 2012)), they were the only measured parameter that was consistently able to clearly detect the sewage plume.

The spatial domain of the model was constrained to 800 m long (x) by 200 m across (y), such that (1) the most heavily polluted sediment, which has been shown to be within several hundred meters of the outfalls (Diaz, 1992; Dinn et al., 2012b; Krogh et al., 2017; CRD, 2014), is within the spatial domain of the model, and (2) so that the water column dilution of sewage was minimal due to the small spatial scale. Thus, we simulate the largest reasonable O_2 deficit.

The lower box was flushed by horizontal advection with water that has properties ($T_{env\ lower}$, $S_{env\ lower}$, $O_{2\ env\ lower}$; Appendix Table A.2) closely matching the summer means observed by instruments on the outfall mooring (Section 4.1.2). The upper box was flushed at the same rate as the lower box, but with the observed warmer and fresher upper 40 m of the water column (Section 4.1, Fig. S1). Because tidal currents are cyclic, carrying material out of the model domain and then back in, the rate of flushing was determined by the summer net daily transport (daily sum of hourly current velocity observations) observed by the Macaulay Point mooring (v_x & v_y, Table 1b, Figs. S2 & S3). This approximation yields the non-tidal or residual currents, which are significantly slower than tidal currents. This assumption is conservative and increases any O_2 deficits. The model boxes are aligned such that the primary axis of the summer currents (south-east, 110°) is parallel with the long axis of the boxes. S was converted to Absolute Salinity on the TEOS-2010 scale (McDougall and Barker, 2011). For the conditions near the outfall, the conversion is nearly 1:1.

The upper box's O_2 concentration, $O_{2\ upper}$, was fixed at 175 mmol m^{-3} (~170 μmol kg^{-1}), a frequently observed value at 40 m depth (Fig. S1). The fixed O_2 concentration in the upper box acts as an additional source of O_2 to the lower box through vertical mixing (M_z). O_2 sources of primary production and atmospheric gas exchange were implicitly modelled by the fixed O_2 concentration in the upper box.

3.2.2. Oxygen depletion

Oxygen depletion in the water column due to a sewage outfall occurs in two steps. First, the dilution of the ambient O_2 with anoxic sewage (sewage system has elevated levels of H_2S, CRD, 2014) creates an immediate drop in dissolved oxygen. Following this initial decline in nearfield oxygen concentration, organic material (DOC and POC) within the sewage is degraded by microorganisms (modelled implicitly), according to first order kinetics with rate constant *k* (common to both DOC and POC for our model) and a temperature-correcting coefficient θ (Tchobanoglous and Burton, 1991). Raw sewage is relatively labile, compared to marine-derived organic matter (k ~ 0.005–0.2 day^{-1}; Ianson and Allen, 2002) with respiration rates up to 0.7 day^{-1}.

Thus, oxygen consumption is the product of the sewage flow rate (F) and the sewage's biochemical oxygen demand (BOD, measured in mmol m^{-3}). This oxygen demand was expressed over time according to its respiration rate (0.7 day^{-1} in the base case). Because currents at the study site are so strong, dilution continues indefinitely, so, unlike a river system which may experience maximum oxygen deficits well downstream of the wastewater discharge (Tchobanoglous and Burton, 1991), we expect the largest oxygen depletion close to the outfall where water column concentrations of sewage are highest and sewage particles are able to settle to the seafloor in significant quantities. These particles enrich the sediment within about 600 m of the outfalls (Krogh et al., 2017; Diaz, 1992; CRD, 2014) and therefore increase the local oxygen demand.

We simulated three size classes of sewage derived organic carbon based on the behaviour of sewage discharge observed by an ROV outfall inspection dive (Krogh, 2017). The first type (DOC_{upper} and DOC_{lower}) is operationally dissolved, (i.e. it moves freely with the currents). The second type ($POC_{suspended}$) consists of small sewage particles which sink and become suspended in the bottom boundary layer, moving along the seabed at a much-reduced speed, which we modelled via a fractional reduction in the ambient current speed (*d*). Lastly, the largest and densest organic carbon particles ($OC_{sediment}$) quickly sink to the bottom of the seabed and are not re-suspended. Because we assumed steady state, $OC_{sediment}$ was instantaneously oxidized in a reflective boundary layer (Bianucci et al., 2011). Natural marine pools of DOC and POC were not simulated because they are assumed to be unaffected by the sewage and thus would have no impact on the size of the oxygen deficit caused by the sewage (i.e. in both model runs with and without sewage, the natural sources would be the same). See Appendix A for the equations governing the model.

Primary treatment (settling tanks and grease skimmers) is able to reduce the BOD of wastewater by 25–40% (Tchobanoglous and Burton, 1991), so one could assume that up to 40% of the Victoria's wastewater BOD load is in the form of suspended sewage particles ($POC_{suspended}$) or sediment ($OC_{sediment}$). However, because the ambient environment around Victoria's sewage outfalls is much higher energy than a settling tank, we assumed that a relatively larger fraction of the wastewater's BOD (at least 80%) is in the functionally dissolved phase (DOC, Appendix Table A.1). Although the ROV video does not allow for the quantification of settling rates, it does confirm that some settling of sewage particles occurs. Thus, we limited our simulations to $POC_{suspended}$ making up 5–15% of the total BOD load and true sediment ($OC_{sediment}$) making up 1–5% (Appendix Table A.1). Despite these two pools of sewage-derived organic material only making up at most 20% of the total sewage organic load, they have longer residence times near the outfalls and therefore exert a disproportionately large impact on both the predicted oxygen deficit and DIC enrichment (Section 4.2).

Table 1b
Physical dimensions and prescribed physical advection and mixing.

Name	Symbol	Units	Sensitivity range	Base case
Horizontal long dimension	x	m	800	800
Horizontal cross dimension	y	m	200	200
Trapping depth (measured downward from the surface)	D_{Trap}	m	0–40	40
Daily net long direction advection	v_x	m day^{-1}	4500–9200	4500
Daily net cross direction advection	v_y	m day^{-1}	900–3400	900
Daily net vertical mixing	M_z	m day^{-1}	1–10	5

4. Results and discussion

4.1. Observational

4.1.1. Vertical profiles

All vertical CTD-O_2 profiles collected near the sewage diffusers illustrated minimal stratification associated with the strong tidal currents in the area. Upon visual examination of nearly 800 profiles, only six profiles showed any evidence of a sewage plume layer; that is, a layer that is fresher, warmer, more turbid, and lower in oxygen than the layers directly above and below it. From within the small subset of profiles that did show plume effects, the largest declines in oxygen were close to sensor accuracy, at < 5 μmol kg^{-1} (Fig. S4). An oxygen decrease of this magnitude would be expected to depress pH by roughly 0.01 units (assuming an associated DIC enrichment of 4 μmol kg^{-1}, fixed TA of 2125 μmol kg^{-1}, S of 32, and T of 10 °C). Despite the lack of oxygen deficits, the concurrent bacteriological data frequently showed high fecal coliform concentrations of up to 6000 colony forming units (CFU) per 100 mL (compared to background levels of < 20 CFU 100 mL^{-1} in surrounding waters) in the mid and deep layers of the water column (CRD, 2014). Post screening but before the sewage is discharged, fecal coliform levels can approach 6000,000 CFU 100 mL^{-1} (CRD, 2014). The typical marine environmental concentrations observed at the monitoring stations thus represent dilution ratios of several thousand to one or greater. However, dilution rates were highly variable, with the lowest observed dilution rates of around 500:1 occurring about once per year (~0.5% of observations).

4.1.2. Moorings

Our data show the full seasonal cycle of O_2, not only at the mooring outfall site, but also in JdF. Although the general seasonal cycle has long been known from ship surveys (Herlinveaux and Tully, 1961; Johannessen et al., 2014; Masson, 2006), the mooring dataset (Fig. 3) reveals significant temporal detail than was previously unknown.

The outer moorings (JdF-W and JdF, orange and green Fig. 3) are heavily influenced by large scale summer coastal upwelling that occurs along the western coast of North America. Upwelled water enters the bottom landward flowing layer of JdF (Fig. 1c), causing lower O_2, lower T, and higher S during the summer (Fig. 3). The inner moorings, located at Boundary Passage (BNDYP, gray, Fig. 3) and at the outfall site (red, Fig. 3), show less influence of upwelled waters and more of waters originating in the SoG, though with oxygen minima still occurring in summer. The mooring located at the eastern entrance to JdF (JdF-E, blue) shows a mixture of both the inner and outer water. In winter, downwelling predominates along the outer coast, causing O_2 and T to rebound at JdF-W. Intense winter storms combined with lower Fraser River discharge produces periodic estuary flow reversals (Thomson et al., 2007), causing surface waters to flow landwards and deep waters to flow towards the Pacific. These reversals likely cause the periodic drops in S seen in winter at JdF-W and JdF (Fig. 3). When compared with the other moorings (Fig. 3), the outfall site has the most oxygen throughout the time series (mean of 183 μmol kg^{-1} even relative to BNDYP's mean of 172 μmol kg^{-1}).

Acoustic ocean current observations by the outfall mooring agree with those of past mechanical current meters (Chandler, 1997), showing a dominant current direction to the south-east (110°), particularly in summer (Figs. S3). The dominant current direction is part of the larger scale estuarine exchange and suggests that at least some of the sewage may be carried within the bottom layer around Victoria's waterfront and towards Haro Strait. This observation is contrary to the assumption that the sewage outfalls are shallow enough to ensure that all of the sewage is immediately carried towards the Pacific Ocean in the outward flowing surface layer (Chapman, 2006). However, even if some sewage is able to enter Haro Strait from JdF, the majority of it would likely be mixed into the surface layers and subsequently advected back to the Pacific Ocean (Pawlowicz et al., 2007) (Fig. 1c).

The temporal resolution of the outfall mooring reveals the highly variable nature of bottom layer oxygen near the outfall in all seasons (wide frequency distributions, Fig. 4). During the summer, when dissolved oxygen is lowest (Figs. 3 and 4) and water column stratification increases (Krogh, 2017) dramatic shifts in oxygen are commonly observed. A single tidal cycle can cause oxygen to vary by nearly 100 μmol kg^{-1} (Fig. 5a). Despite these dramatic changes, oxygen levels were always observed to be well above the 62 μmol kg^{-1} (2 mg L^{-1}) hypoxic threshold (Hofmann et al., 2011; Fig. 4). However, because cold water can hold more oxygen than warm water, the percent saturation of oxygen did, for brief periods (0.07% of the whole time

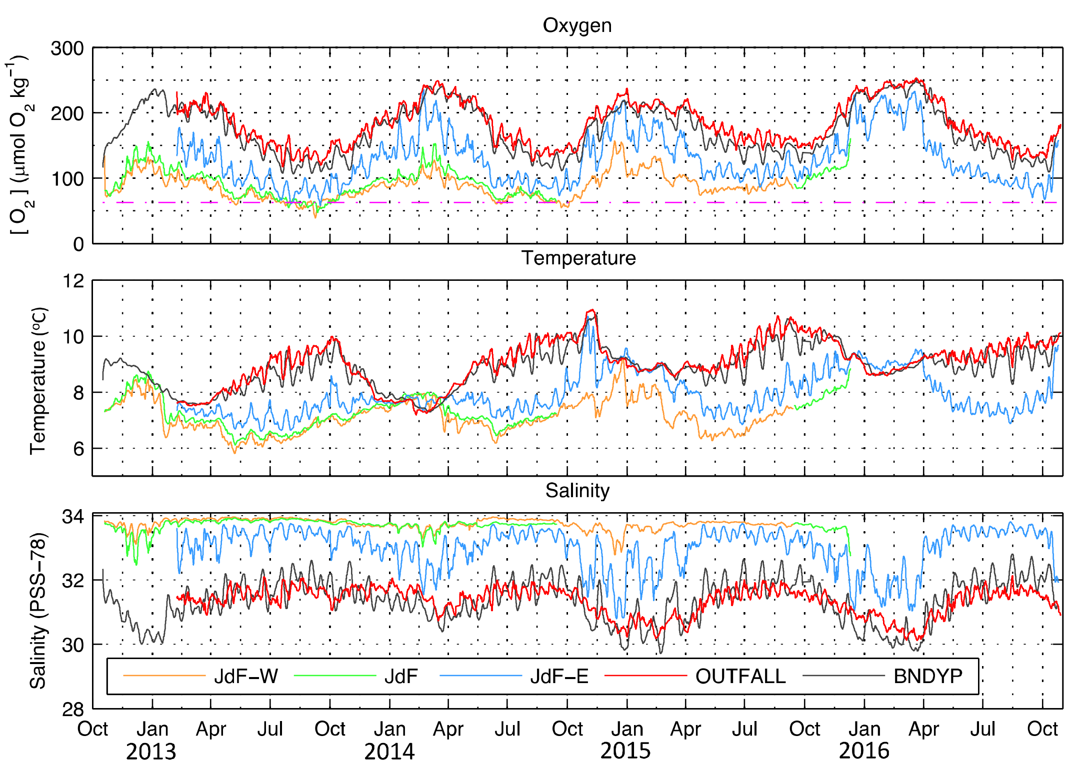

Fig. 3. Time series of oxygen concentration, temperature, and salinity from the four-year mooring dataset filtered with a 25-hour running mean to remove semi-diurnal and diurnal tidal effects. The horizontal dashed magenta line indicates a hypoxic threshold of 62 μmol kg^{-1} (Hofmann et al., 2011). All moorings are anchored to the bottom with instruments approximately 6 m off the seabed. Depths of each mooring are shown in Fig. 1c.

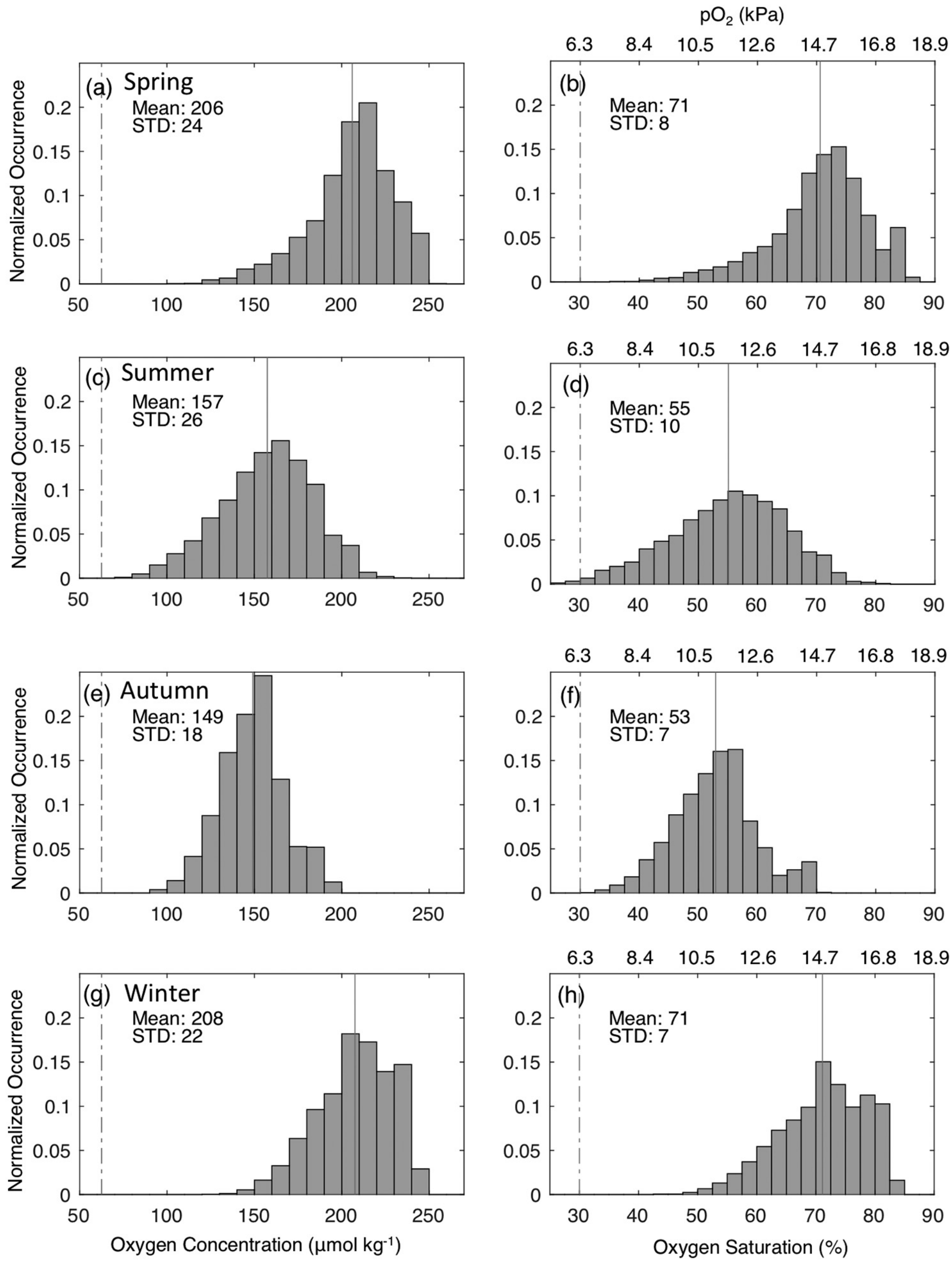

Fig. 4. The left column shows histograms (probability density functions) of hourly oxygen observations at the outfall mooring, while the right column shows the same information expressed as percent saturation on the bottom x-axis and partial pressure of O_2 on the upper x-axis. The means (vertical solid line) and standard deviations (STD) in the upper left corner of each plot are in units of μmol kg^{-1} in the left panels and percent saturation in the right panels. Hypoxia thresholds are marked by the vertical dashed lines. The four seasons are spring (a,b, day of year 77–137), summer (c,d, 138–225), fall (e,f, 256–314), and winter (g,h 315–76) (Bylhouwer et al., 2013).

series), fall below 30% saturation (pO_2 6.3 kPa, Fig. 4). Saturation states below 30%, especially if persistent, have been shown to have negative impacts on many marine organisms (Hofmann et al., 2011). Autumn (Fig. 4e,f) has a slightly lower mean than summer (149 compared to 157 μmol kg^{-1}) but has less negative skewness resulting in higher minimum concentrations and no observations below 30% saturation. Spring and winter (Fig. 4a,b and g,h) have the highest seasonal mean concentrations and saturation states, as a result of downwelling circulation on the outer coast.

Oxygen and S both follow a tidal pattern at the outfall, best seen in a short period of the hourly time series (Fig. 5a). Flood tides bring higher S and lower O_2, while ebb tides bring lower S and higher O_2. A scatter of the same data (black points Fig. 5b) shows the strong linearity of the S-O_2 relationship with an r^2 of 0.92. The entire summer of 2015 (gray points Fig. 5b) shows more scatter, but the strong linearity remains (r^2 of 0.88). The discharge rate of sewage is highly periodic with two daily peaks resulting from human activities (morning and evening) and two lows (mid-day and overnight) (Figs. S5 & S6). If sewage caused significant O_2 consumption, the scatter above and below the linear best-fit O_2-S relationship would correlate with sewage flow rate, with negative residuals (i.e. O_2 observations lower than the O_2 concentration predicted based on S observations) corresponding to high sewage flow rates. Such a correlation is not observed (Fig. 5c).

Species composition observed by ROV near both outfalls also indicates oxic conditions. Around the diffusers of the Macaulay outfall, spotted ratfish (*Hydrolagus colliei*) were present in high concentrations. Sunflower stars (*Pycnopodia helianthoides*), staghorn sculpin (*Leptocottus armatus*), English sole (*Parophrys vetulus*), and rock fish (*Sebastes* spp.) were also present in significant numbers. At the same time, no squat lobster (*Munida quadrispina*), slender sole (*Lyopsetta exilis*), or bacterial mats were observed, all of which are local species known to inhabit nearby naturally hypoxic environments (Chu and Tunnicliffe, 2015). Species present near Clover Point were different from those seen in such high abundance at Macaulay (e.g. copper rock fish, *Sebastes caurinus*), but again no hypoxic-tolerant species were seen (Krogh, 2017). In the case of the Macaulay outfall where the seabed slopes gently, the ROV video showed expected patterns of high abundance and low diversity near the diffusers, while further away abundance decreased, but diversity greatly increased (Pearson and Rosenberg, 1977).

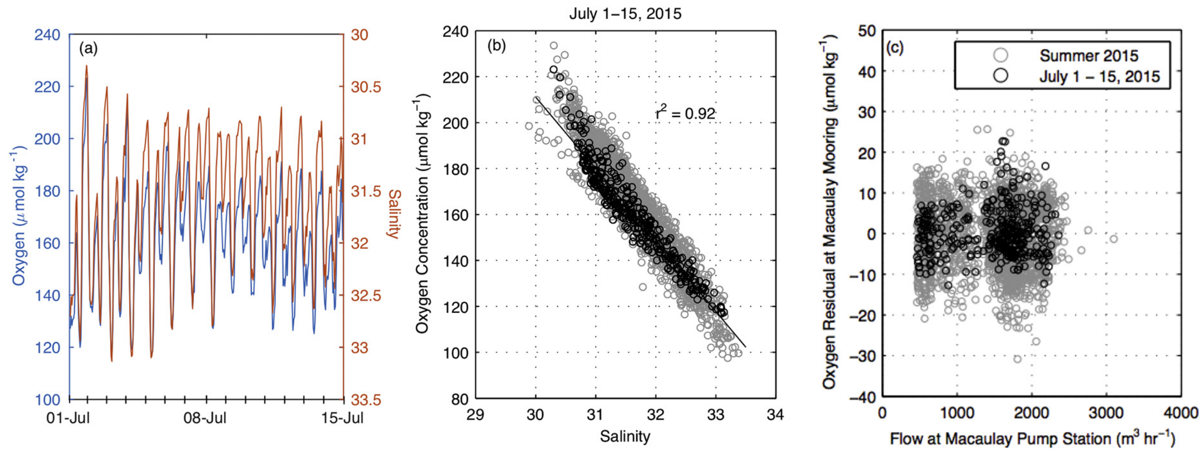

Fig. 5. (a) Hourly time series of salinity and oxygen at the Macaulay Point mooring during July 1–15, 2015 (b) black circles show the same data as (a) on a scatter plot with a linear fit while gray circles are all data from the summer (day of year 138–225) of 2015. (c) Black circles show the oxygen residual after the subtraction of the linear best fit from (b) plotted against the sewage flow rate as measured at the Macaulay pump station. Again the gray circles show the residual after the seasonal best fit line (not shown) is subtracted.

4.1.3. *Water mass analysis*

To compare the conditions observed at the outfall mooring to those expected if no sewage outfalls were present, we determined the properties of source water masses that influence conditions at the outfall mooring. The strong linear relations between S and O_2 (Fig. 5b) and between S and T (Fig. 6a) indicate that only two source water masses contribute to the variability near the outfall. Masson (2006) conducted an optimum multi-parameter water mass analysis of the entire region (SoG, Haro Strait, and JdF). Her analysis showed that the area just offshore from the outfalls was well defined by two source water masses, deep JdF water and surface Fraser River plume water. We define the deep JdF water mass as the average summer (2013, 2014, 2015) properties (T, S, O_2) observed at 225 m by the mooring located at the western entrance of JdF (JdF-West, Fig. 1a). Our results for the deep JdF water mass all closely match those found by Masson (2006) (Table 2).

We found the second end-member that Masson (2006) defined as the Fraser River plume source water to be too cold and fresh to be the other source of water observed at the outfall (Fig. 6a). Instead, we define a unique end-member using data from surface waters along the northern edge of Haro Strait (summers of 2015 and 2016, ferry data zone, Fig. 1a), which itself is made up of a mixture of mostly Fraser River plume and deep JdF waters (Masson, 2006). We assign it the summer (day 138–225) average (T, S, O_2) observed by the ferry system (Section 3.1.3) as it crosses the northern edge of Haro Strait (Fig. 1a). Surface water properties at this location include effects of solar heating and biological oxygen production as the water moves from the Fraser river mouth to Haro Strait (Krogh, 2017). These data fall along a straight line in T-S space connecting the deep JdF water with the Macaulay bottom water (Fig. 6a).

Interannual variability in end-member properties was generally low, with most seasonal means falling within the range defined by the respective standard deviations (Table 2). However, conditions at JdF-W did change significantly. Between summer 2013 and 2015, S declined by 0.14 (mean seasonal variability 0.02), O_2 rose by 15 μmol kg^{-1} between summer 2013 and summer 2015 (mean seasonal variability 6 μmol kg^{-1}) and T rose by 0.4 °C (mean seasonal variability of 0.2 °C). A regional scale warming event, known as 'The Blob' (Bond et al., 2015), influenced the mooring network after November 2014 and contributed to the general warming trend seen throughout the time series (Fig. 3). It is therefore likely that the summer mean T in the surface of N-Haro were slightly cooler in 2013 and 2014 (for which no ferry data are available) compared to those observed in summers of 2015 and 2016.

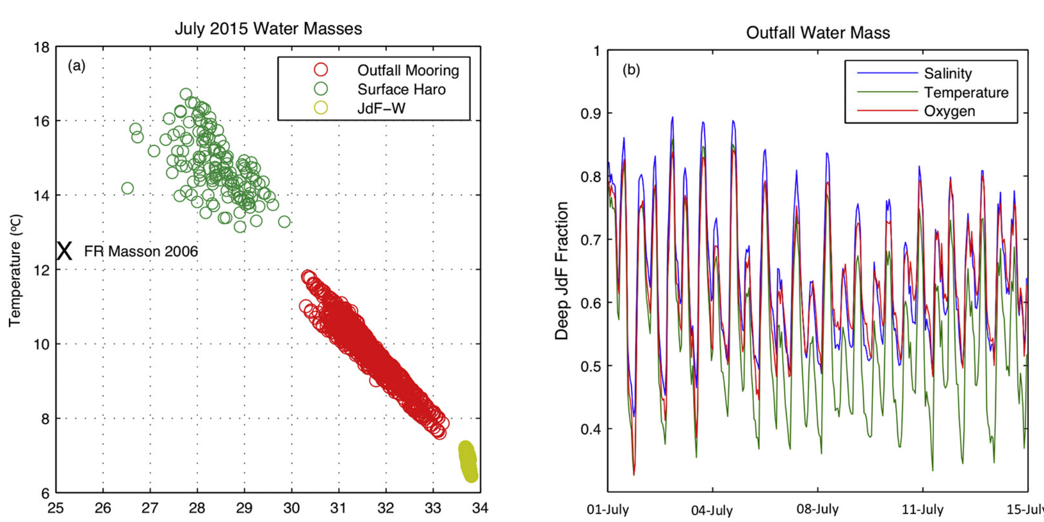

Fig. 6. (a) Temperature vs salinity for the two source water masses (green and yellow) from July 2015 and the outfall mooring water (red). Mooring data points (red outfall and yellow JdF-W) are hourly data while the ferry data (green) is one point per crossing of the ferry data area (Fig. 1a). Masson's (2006) Fraser River end member is also marked. (b) The fraction of deep JdF water at the outfall mooring calculated from each of the three parameters (T, S, O_2).

Table 2
Summer (year-day 138–225) mean and standard deviations for the two end-member water masses. DIC data used for end-members were collected between 2010 and 2012 while TA data were collected in 2003 and 2010–2012. Predicted pH calculations were made using CO2SYS and a Monte Carlo simulation of n = 1000 was used to calculate uncertainty. *Ferry data from the summer of 2015 was only available for July. The predicted pH for 2016 JdF-W end-member used the average summer T and S values from 2013 to 2015.

Mean summer JdF-W					
	2013	2014	2015	2016	Masson, 2006
Salinity (PSS-78)	33.91 ± 0.03	33.90 ± 0.03	33.77 ± 0.04	–	33.9
Temperature (°C)	6.3 ± 0.1	6.7 ± 0.2	6.7 ± 0.3	–	6.4
Oxygen (μmol kg^{-1})	69 ± 7	73 ± 8	84 ± 4	–	78
Estimated DIC (μmol kg^{-1})	2250 ± 4	2250 ± 4	2250 ± 4	2250 ± 4	–
Estimated TA (μmol kg^{-1})	2271 ± 4	2271 ± 4	2271 ± 4	2271 ± 4	–
Calculated pH	7.63 ± 0.02	7.62 ± 0.02	7.62 ± 0.02	7.62 ± 0.02	–
Mean summer N-Haro surface (ferry data)					
	2013	2014	2015*	2016	
Salinity (PSS-78)	–	–	28.2 ± 0.7	27.8 ± 0.7	–
Temperature (°C)	–	–	13.5 ± 1.4	13.1 ± 1.1	–
Oxygen (μmol kg^{-1})	–	–	291 ± 30	291 ± 26	–
Estimated DIC (μmol kg^{-1})	–	–	1870 ± 23	1843 ± 25	–
Estimated TA (μmol kg^{-1})	–	–	1979 ± 40	1958 ± 39	–
Calculated pH	–	–	7.9 ± 0.1	7.9 ± 0.1	–
Outfall mooring summer conditions					
	2013	2014	2015	2016	–
Salinity (PSS-78)	31.6 ± 0.6	31.6 ± 0.6	31.6 ± 0.6	31.6 ± 0.6	–
Temperature (°C)	8.9 ± 0.7	9.3 ± 0.7	9.5 ± 0.9	9.4 ± 0.7	–
Oxygen (μmol kg^{-1})	153 ± 25	167 ± 30	164 ± 23	166 ± 23	–
Calculated TA (μmol kg^{-1})	–	–	2153 ± 40	2162 ± 36	–
Calculated DIC (μmol kg^{-1})	–	–	2102 ± 49	2110 ± 44	–
Calculated pH	–	–	7.72 ± 0.07	7.72 ± 0.07	–

In addition, we estimated DIC and TA end-members for deep JdF and N-Haro surface from the comparatively sparse data available in the region. For the deep JdF, DIC is 2250 ± 4 μmol kg^{-1} (Ianson et al., 2016). Since the ferry system did not measure inorganic carbon, the N-Haro surface end-member requires the additional step of interpolation between the surface SoG and deep JdF to obtain the same S as N-Haro surface. Although Ianson et al. (2016) reported a surface ~15 m integrated Fraser-plume DIC end-member, the T-S associated with that water mass is colder and fresher than the line formed by N-Haro surface and the deep JdF (Fig. 6a). However, the surface data (S > 20, not during freshet; data under ~5 m excluded) do fall roughly on this T-S line. Thus, we define a surface-SoG DIC end-member as 1570 ± 70 μmol kg^{-1} (at S = 23.6 ± 0.4) with the large uncertainties due to both strong inter-annual and shorter term variability in surface properties. TA was determined from regional TA-S regression from the Ianson et al. (2016) data ($51 * S + 532$; S > 20).

Using the water masses defined in Table 2 and assuming that these are the only two source water masses, the average summer mixing fraction of deep JdF water at the outfall mooring was calculated for each of the three measured variables (Krogh, 2017).

Differences in mixing fractions between the three variables would indicate non-conservative behaviour (such as oxygen being consumed by sewage discharge) or incorrect end-member properties; however, they all agreed within their estimated uncertainties (Table 3). This overall agreement between the predicted mixing fractions indicates that no large oxygen deficit is occurring at the outfall mooring; however, the resolution of this method is not good enough to rule out the possibility of a modest oxygen deficit (< 15 μmol kg^{-1}).

In addition to seasonal mean mixing fractions, we used the hourly resolution of the outfall mooring to calculate the hourly water mass fractions (Fig. 6b). These calculations show that there is generally good temporal agreement between T, S and O_2 (Fig. 6b). For brief periods during flood tides, the fraction of deep JdF water found at the outfall can exceed 85%. At these times, the outfall area is most at risk of hypoxia. If oxygen in deep JdF water were to fall to 23 μmol kg^{-1} while N-Haro surface water maintained its current level of oxygenation, which is likely given the energetic mixing in the area (Ianson et al., 2016), short term (several hours or less) flood tide hypoxia (< 62 μmol kg^{-1}) at the outfall site and surrounding area would be expected (star in Fig. 7). Declines in bottom oxygen at the mouth of JdF have been observed over the past thirty years (Crawford and Peña, 2013). Although the drivers of this oxygen decline are not fully understood and may be oscillatory in nature (Crawford and Peña, 2016), if oxygen concentrations were to continue to decline at the current rate of 0.83 μmol kg^{-1} y^{-1}, suggested by Crawford and Peña (2013), oxygen in the deep water of JdF could fall below 23 μmol kg^{-1} by the 2050s.

Table 3
Mixing ratios predicted based on the source water properties of Table 2 and the conditions observed at the outfall mooring. Due to incomplete data sets the N-Haro surface observations from summer 2015 are applied to 2013 and 2014. Likewise, the JdF-W 2016 data are taken to be the same as the 2015 observations. Only 2015 has complete data from both the N-Haro surface and JdF-W.

Mean summer deep Juan de Fuca fraction at the outfall mooring				
	2013*	2014*	2015	2016*
Salinity (PSS)	0.59 ± 0.05	0.60 ± 0.05	0.62 ± 0.05	0.63 ± 0.05
Temperature (°C)	0.64 ± 0.08	0.62 ± 0.09	0.59 ± 0.10	0.58 ± 0.10
Oxygen (μmol kg^{-1})	0.62 ± 0.07	0.57 ± 0.08	0.61 ± 0.06	0.60 ± 0.06

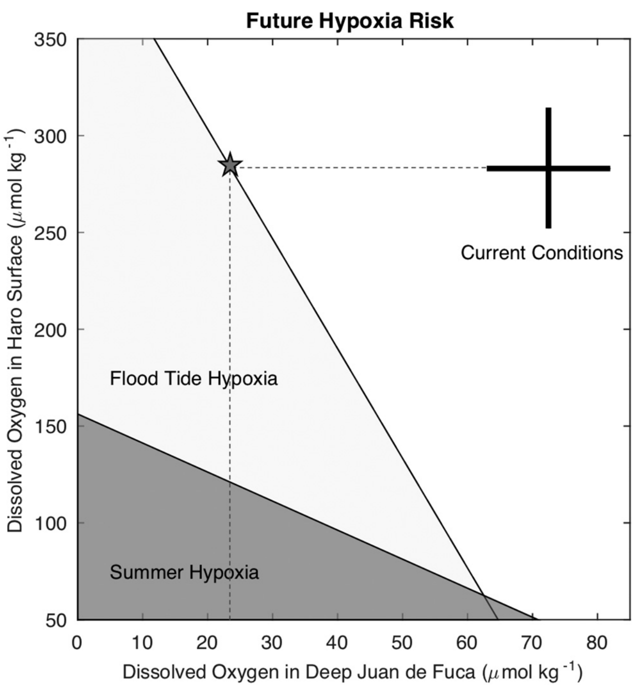

Fig. 7. Hypoxia (< 62 μmol kg^{-1}) risk at the outfalls and surrounding region from the potential declines of oxygen in the source water masses, assuming the ratio of source water masses does not change in the future. The light gray area represents the combination of conditions required to give short term (hourly) hypoxia during summer flood tides (85% deep JdF water). The dark gray area represents the combination of conditions required to give summer seasonal hypoxia (60% deep JdF water). Current summer means and standard deviations from the N-Haro surface and deep JdF (Table 2) are marked by the cross in the upper right. The star marks the onset of flood tide hypoxia if N-Haro waters do not change. The horizontal and vertical scales are different.

Oxygen concentrations this low in deep JdF would put the near bottom environment around the outfalls (and throughout the JdF region) at risk of short term hypoxia, but, not as a result of the sewage discharge.

If the oxygen content of N-Haro surface waters were also to change, a variety of end-member oxygen combinations could lead to flood tide hypoxia (light gray area in Fig. 7). Climate change will likely raise the surface temperatures in N-Haro surface waters (Mote and Salathé, 2010) and in so doing reduce the amount of oxygen in these waters (Johannessen and Macdonald, 2009). Assuming no change to the mean summer oxygen saturation, currently 108% (Table 2) at the ferry crossing (calculated with Garcia and Gordon, 1992, 1993), a + 2 °C increase in surface temperature in N-Haro surface would result in a decrease in N-Haro surface oxygen concentration from 291 to 279 μmol kg^{-1}. Under such conditions, deep JdF water needs to maintain oxygen levels above 25 μmol kg^{-1} to avoid the risk of flood tide hypoxia (62 μmol kg^{-1}) at the outfalls compared to 23 μmol kg^{-1} required at today's temperatures. With +4 °C of surface N-Haro warming (a further decline of surface dissolved oxygen to 269 μmol kg^{-1}), deep JdF water needs to maintain oxygen levels above 27 μmol kg^{-1} to avoid risk of flood tide hypoxia. Thus, the oxygen concentration at the outfalls is relatively insensitive to significant temperature increases in N-Haro surface waters.

Seasonally, the average summer deep JdF fraction hovers around 60% (Table 3). Even in the most extreme case if the deep JdF water were to become anoxic, 40% of the water at the outfall sites comes from the surface of N-Haro, which has a summer seasonal average oxygen concentration of 291 μmol kg^{-1}. Thus, to reduce the mean oxygen concentration at the outfalls below 62 μmol kg^{-1} (dark gray area in Fig. 7), oxygen in the surface waters of N-Haro Strait would need to fall by > 130 μmol kg^{-1}, an extremely unlikely scenario. Even with a changing climate, the powerful tides in Haro Strait will maintain high levels of oxygenation (Johannessen et al., 2014; Ianson et al., 2016).

4.1.4. Inorganic carbon and total alkalinity

Dissolved inorganic carbon (DIC) and total alkalinity (TA) samples (colored diamonds, Fig. 8a) collected from the outfall monitoring stations (Fig. 1c) overlap with previous observations from JdF and Haro Strait (Ianson et al., 2016). As the organic carbon within the sewage is respired it would be expected to raise DIC and lower TA (Emerson and Hedges, 2008; Moore-Maley et al., 2016); however, our observations show no evidence of such a shift. This result is consistent with the finding by Johannessen et al. (2015) that municipal sewage outfalls do not significantly contribute to the regional (SoG and JdF) carbon budget.

Nearly all of the samples collected in November 2015 (blue), July 2016 (red), and January 2017 (cyan) were below a pH of 7.8 and corrosive to aragonite (saturation state, $\Omega_A < 1$) (Fig. 8b,c). The presence of corrosive near-surface waters is common in the area (Feely et al., 2010; Ianson et al., 2016). The July 2015 (green) samples stand out in this regard as they show aragonite supersaturation throughout

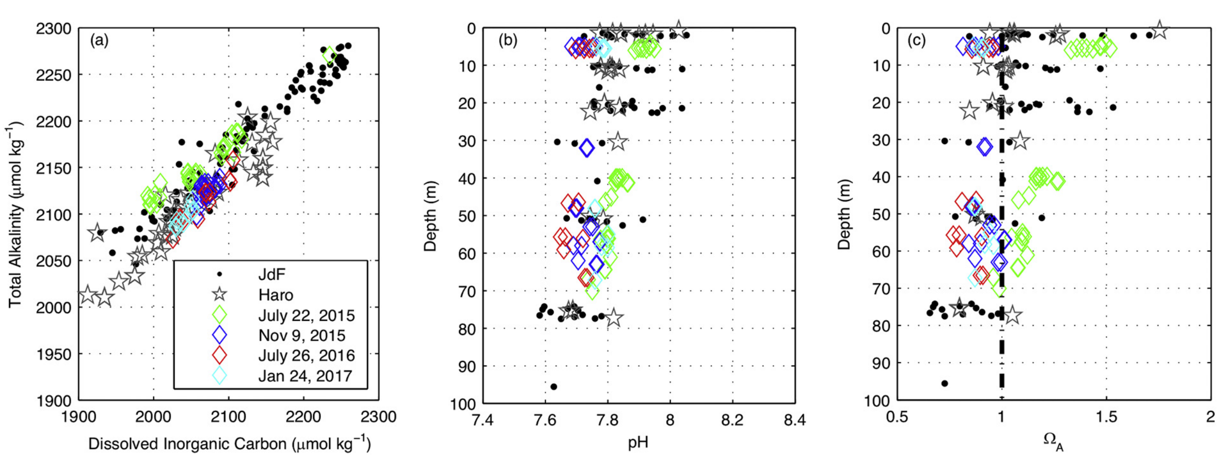

Fig. 8. (a) Comparison of total alkalinity vs. dissolved inorganic carbon collected near the outfall sites (colored diamonds) with past observations from JdF (black dots) and Haro Strait (gray stars) (Ianson et al., 2016). (b) Depth vs. calculated pH from CO2SYS. (c) Depth vs. aragonite saturation state Ω_A calculated from CO2SYS (van Heuven et al., 2011).

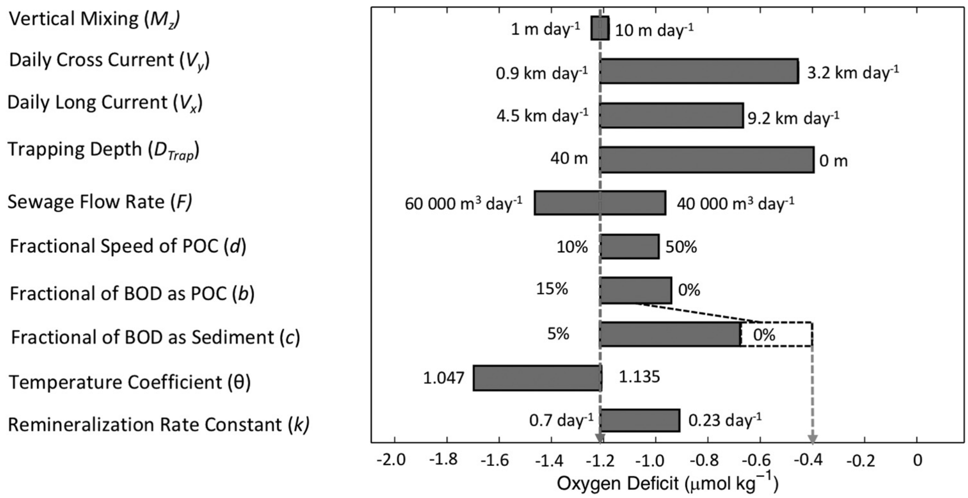

Fig. 9. Sensitivity of final model result to various parameters. The left vertical arrow represents our base case (Table 1a and Appendix Table A.1), a conservative yet plausible scenario of current sewage flow rates, ocean currents, a deep trapping depth, and a high estimate of sedimentation. The right vertical arrow shows the approximate oxygen deficit if all POC and sediment organic carbon were removed from the sewage. All parameters are varied independently in relation to the base case.

the water column, likely due to summer biological draw-down of DIC.

Using DIC and TA water mass end-members (Table 2) we calculated the daily DIC, TA and pH variability at the outfall from observed S (Ianson et al., 2016). Although large diurnal variations are predicated to occur in both DIC and TA (up to approximately 150 μmol kg^{-1} day^{-1}), they largely serve to cancel one another out, and pH is predicted to be relatively stable, varying by up to 0.1 pH units over the course of the day. The minimal variability in predicted pH at the outfall occurs because the SoG is enriched in DIC relative to outer waters (Ianson et al., 2016). Therefore, while N-Haro contributes high O_2 to the area around the outfall, it does not serve to significantly dilute or reduce DIC.

4.2. Model

Running the model with conservative, yet plausible, estimates of input parameters (base case Table 1b and Appendix Table A.1) resulted in a predicted O_2 deficit of only 1.2 μmol kg^{-1} in the lower box due to sewage (red arrow, Fig. 9). Correspondingly, an O_2 deficit of this magnitude would be expected to raise DIC by 1.0 μmol kg^{-1} (DIC:O_2 ratio of 0.8), drop TA by 0.2 μmol kg^{-1}, and depress pH by 0.004 (assuming S of 32 and T of 10 °C). These model results agree with our observations. Some O_2 depletion and carbon enrichment is likely occurring in the immediate vicinity (10s to 100 s of m) of the outfalls, but their magnitudes are both so small, in comparison to natural variability, that they are effectively undetectable. The reason impacts are so minimal is the short physical residence time (for the freely moving DOC, 2.4 h) due to strong currents and subsequent export of the majority (base case, 93%) of unoxidized DOC from the model domain. Suspended sediment ($POC_{suspended}$) and true sediment ($OC_{sediment}$), however, have much longer or infinite (for sediment) residence times and enrich the nearfield sediment with organic carbon (Diaz, 1992), resulting in an estimated average sediment O_2 demand of 0.1 mol m^{-2} day^{-1} over the 200 × 800 m model domain. Running the model with primary treatment in place ($POC_{suspended}$ and $OC_{sediment}$ set to zero), cuts the already small O_2 deficit by > 60% to only 0.4 μmol kg^{-1} (green arrow, Fig. 9).

Our estimate of the O_2 deficit due to the sewage is most sensitive to the trapping depth (the depth above which sewage does not rise) and the horizontal advection rates (Fig. 9). In reality, these parameters are not independent of one another. Conditions that yield high horizontal advection rates will trap the plume deeper in the water column (deeper trapping depth, less sewage dilution in the vertical) but also reduce the residence time within the model domain (Li and Hodgins, 2004). Currents in the area are dominated by tides and are not at risk of changing in the future. The tidal currents alone are strong enough to spread the effluent out over a large area of several hundred square kilometers within a few tidal cycles, representing roughly 10^{10} m^3. If all of Victoria's sewage were completely mixed and respired within this volume, the O_2 demand would be only 0.06 μmol kg^{-1} day^{-1}.

4.2.1. Future scenarios

As the population of greater Victoria grows, so too will the amount of sewage needing disposal. However, even if the current rate of sewage discharge is doubled or even quadrupled, the predicted O_2 deficits are still small at −2.4 and −4.8 μmol kg^{-1} respectively. Warming would increase the respiration rates of bacteria and thus the local O_2 deficit. However, because residence times are short, increasing rates of respiration have little impact: −1.3 μmol kg^{-1} at +2 °C and −1.5 μmol kg^{-1} at +4 °C compared with −1.2 μmol kg^{-1} at current temperatures.

Victoria's location next to such a highly energetic marine environment is not common. Neighbouring cities in the Salish Sea such as Vancouver, BC and Seattle, Washington face different physical conditions. Iona, one of Vancouver's main sewage outfalls discharges into an environment with peak currents speeds roughly 1/10th those at Macaulay Point (Dinn et al., 2012a). If net daily current speeds around Victoria were reduced to this level, the residence time within the model would increase from a few hours to a few days, increasing O_2 deficits to over 20 μmol kg^{-1} and reducing pH by 0.07 units (DIC +16 μmol kg^{-1}, TA −4 μmol kg^{-1} at S of 32 and T of 10 °C). O_2 deficits this large would lead to significant periodic hypoxia (< 62 μmol kg^{-1}) around Victoria's outfalls. Similarly, peak current speeds near Seattle are about one third of those near Victoria (Bretschneider et al., 1985). If Victoria's net daily current speeds were reduced to this level it would likely more than quadruple Victoria's O_2 deficit to just over 5 μmol kg^{-1} (corresponding pH drop of 0.02 units). In addition, Seattle and Vancouver are not adjacent to tidal narrows. Victoria's proximity to the strong consistently well ventilated Haro Strait region provides significant subsurface O_2 injection.

Greater Victoria's plan for moving to tertiary treatment (secondary with disc filtration) by 2020 includes combining the flows from Clover and Macaulay Points into one central outfall to be built between the two existing ones (treated flows up to 108,000 m^3 day^{-1}, CRD, 2017). If the proposed plant is built, effluent quality will be vastly improved

(> 85% reduction in total organic loadings and an almost total elimination of total suspended solids) (CRD, 2017). The combination from two outfalls to one is unlikely to produce significant O_2 depletion due to improved effluent quality. However, if the length of the new outfall is shorter than the current deep-water outfalls (60–65 m depth and 1.2–1.6 km offshore), it will be less effective at dispersal (Li and Hodgins, 2010). There would be less vertical space available to mix the effluent, and currents are likely slower closer to shore due to frictional drag (and possibly directed towards shore at times). A plant failure in this situation, if effluent could not be redirected to the old Clover and Macaulay outfalls, would pose a greater risk than the current system. Even with a plant failure, O_2 depletion is still likely to be small (~3 μmol kg^{-1}), but larger than what is currently experienced.

5. Summary and conclusions

Our work builds on that of others (Chapman et al., 1996; Dinn et al., 2012b; Johannessen et al., 2015; Puente and Diaz, 2015), showing the importance of the receiving environment when determining the negative impacts of municipal sewage outfalls. Treating all wastewater to the same level will not result in consistent environmental protection, as some receiving environments are much more sensitive than others. Victoria's marine environment has several unique mitigating factors: strong and cold tidal currents rapidly dilute the sewage while slowing respiration, highly oxygenated N-Haro Strait surface waters make up a significant portion (~40%) of the water near the outfalls, and the whole region is so well mixed that primary production is light limited year round (Mackas and Harrison, 1997). These features give the marine environment around Victoria a high assimilative capacity for organic waste. Unlike many areas, higher levels of treatment in Victoria will have a nearly unobservable impact on O_2 and DIC.

Our results show that the waters surrounding Victoria's sewage outfalls are highly oxygenated at present, with annual minimums occurring in summer (seasonal summer average 158 μmol kg^{-1}). O_2 concentrations were always observed to be above hypoxic (< 62 μmol kg^{-1}) thresholds (lowest observation 75 μmol kg^{-1}, 30% saturation). Water column pH near the outfalls varied from a low of 7.65 near the bottom to 7.95 near the surface, not unusual for this area (Ianson et al., 2016). The concentration of O_2 at the Macaulay Point outfall mooring varied greatly with the tides and the mixing of two source water masses (deep JdF and surface N-Haro). When compared to the large natural variability, the impacts of the outfalls on O_2, DIC, and pH are negligible. A simple steady state model of the system that employed conservative estimates of input parameters predicted a nearly unobservable 1.2 μmol kg^{-1} O_2 deficit and a 1.0 μmol kg^{-1} DIC enrichment (pH decrease of 0.004) attributable to the sewage over a small area of 0.16 km^2 surrounding the Macaulay outfall. Although the Clover Point outfall was not explicitly modelled it is assumed to have an even smaller impact on O_2 due to its higher energy environment. If neighbouring Pacific shelf slope water that flows into this region continues its long term decline in dissolved O_2 (Crawford and Peña, 2013), hypoxia in the entire sub-surface waters of JdF including the area surrounding Victoria is possible by the 2050s.

Acknowledgments

We thank Marty Davelaar for the analysis of our carbon samples, Shirley Lyons for providing field support and sharing past data collected by the CRD, Ken Denman and Sophia Johannessen for their helpful comments on the manuscript, Ocean Networks Canada for data support as well as the captain and crew of the *MSV John Strickland*. Funding was provided by a NSERC Industrial Postgraduate Scholarship (#477944) to J. Krogh, the Capital Regional District Environmental Protection Division, Debby Ianson was supported by Fisheries and Oceans Canada. None of the funding sources influenced the study design, data analysis, data interpretation, or the decision to publish. The Capital Regional District was involved in sample collection near outfalls owned by them.

Appendix A

The model is described in Section 3.2 with fluxes illustrated in Fig. 2. Model parameters (Table A.1), full equations, and boundary conditions (Table A.2) are presented below.

Table A.1
Biological model parameters and anthropogenic forcing.

Name	Symbol	Units	Sensitivity range	Base case	Reference
Sewage flow rate	F	m^3 day^{-1}	40,000–60,000	50,000	CRD, 2014
Sewage carbonaceous biochemical oxygen demand	CBOD	mmol m^{-3}	7600	7600	CRD, 2014
Sewage biochemical oxygen demand	BOD	mmol m^{-3}	8500	8500	CRD, 2014
Sewage temperature	T_{sewage}	°C	20	20	CRD, 2014
Sewage salinity	S_{sewage}	kg m^{-3}	0	0	CRD, 2014
Sewage oxygen	O_{sewage}	μmol kg^{-1}	0	0	CRD, 2014
Sewage molar ratio DIC:O_2	r	–	0.7–0.9	0.8	CRD, 2014
Temperature correction constant	θ	–	1.047–1.135	1.135	Tchobanoglous and Burton, 1991
Sewage decay rate	k	day^{-1}	0.23–0.7	0.7	Tchobanoglous and Burton, 1991
DOC fraction of sewage BOD	a	–	0.80–0.94	0.80	Section 3.1.3, Tchobanoglous and Burton, 1991
POC fraction of sewage BOD	b	–	0.05–0.15	0.15	Section 3.1.3, Tchobanoglous and Burton, 1991
$OC_{sediment}$ fraction of BOD	c	–	0.01–0.05	0.05	Dinn et al., 2012b
Fractional speed of POC	d	–	0.1–0.5	0.1	Section 3.1.3

Model equations

Temperature and salinity in the lower box were simulated according to Eqs. (1) and (2)

$$vol_{upper}\frac{dJ_{upper}}{dt} = HA_{upper}(J_{env} - J_{upper}) + VM(J_{lower} - J_{upper}) \tag{1}$$

$$vol_{lower}\frac{dJ_{lower}}{dt} = HA_{lower}(J_{env} - J_{lower}) + VM(J_{upper} - J_{lower}) + F(J_{sewage} - J_{lower}) \tag{2}$$

where J represents either temperature or salinity and F is the sewage flow rate. Subscript env indicates the environmental concentrations (Appendix Table A.2) of salinity, temperature, and oxygen outside of the model domain while subscript *sewage* indicates the properties of sewage.

$$HA_{upper} = xv_yD_{Trap} + yv_xD_{Trap} \tag{2.1}$$

$$HA_{lower} = xv_y(60 - D_{Trap}) + yv_x(60 - D_{Trap}) \tag{2.2}$$

$$VM = xyM_z \tag{2.3}$$

$$vol_{upper} = xyD_{Trap} \tag{2.4}$$

$$vol_{lower} = xy(60 - D_{Trap}) \tag{2.5}$$

Dissolved oxygen, which was fixed in the upper box (175 mmol m^{-3}), is simulated in the lower box according to Eq. (3)

$$\frac{dO_{2\,lower}}{dt} = \frac{(eqn\ 2)}{vol_{lower}} - k\theta^{(T_{lower}-20)}(DOC_{lower} + POC_{suspended}) - \frac{OC_{sedimemt}}{vol_{lower}} \tag{3}$$

where

$$OC_{sediment} = c*F*BOD \tag{3.1}$$

Dissolved organic carbon, (DOC_{lower} and DOC_{upper}) were simulated in both the upper and lower boxes according to Eqs. (4) and (5) respectively.

$$\frac{dDOC_{lower}}{dt} = \frac{a*F*BOD}{vol_{lower}} + \frac{DOC_{upper}*VM}{vol_{lower}} - \frac{DOC_{lower}*(HA_{lower} + VM)}{vol_{lower}} - k\theta^{(T_{lower}-20)}DOC_{lower} \tag{4}$$

$$\frac{dDOC_{upper}}{dt} = \frac{DOC_{lower}*VM}{vol_{upper}} - \frac{DOC_{upper}*(HA_{upper} + VM)}{vol_{upper}} - k\theta^{(T_{upper}-20)}DOC_{upper} \tag{5}$$

Suspended particles were only present in the lower box and were simulated according to Eq. (6).

$$\frac{dPOC_{suspended}}{dt} = \frac{b*F*BOD}{vol_{lower}} - \frac{d*HA_{lower}*POC_{supended}}{vol_{lower}} - k\theta^{(T_{lower}-20)}POC_{suspended} \tag{6}$$

Table A.2
Prescribed values of state variables at the model's boundaries.

Parameter	Units	Upper layer	Lower layer
T_{env}	°C	12.3	9.5
S_{env}	kg m^{-3}	29.5	31.5
$O_{2\ env}$	mmol m^{-3}	–	150

Appendix B. Supplementary data

Supplementary data to this article can be found online at https://doi.org/10.1016/j.marpolbul.2018.05.018.

References

Balasubramani, A., Howell, N.L., Rifai, H.S., 2014. Polychlorinated biphenyls (PCBs) in industrial and municipal effluents: concentrations, congener profiles, and partitioning onto particulates and organic carbon. Sci. Total Environ. 473–474, 702–713.

Barwell-Clark, J., Whitney, F., 1996. Institute of Ocean Sciences nutrient methods and analysis. In: Canadian Technical Report of Hydrography and Ocean Science. 182 Institute of Ocean Sciences, Sidney, Canada (43 pp.).

Bianucci, L., Denman, K.L., Ianson, D., 2011. Low oxygen and high inorganic carbon on the Vancouver Island Shelf. J. Geophys. Res. Oceans 116, 1–20. http://dx.doi.org/10.1029/2010JC006720.

Bond, N.A., Cronin, M.F., Freeland, H., Mantua, N., 2015. Causes and impacts of the 2014 warm anomaly in the NE Pacific. Geophys. Res. Lett. 42, 3414–3420. http://dx.doi.org/10.1002/2015GL063306.

Bretschneider, D.E., Cannon, G.A., Holbrook, J.R., Pashinski, D.J., 1985. Variability of subtidal current structure in a fjord estuary: Puget Sound, Washington. J. Geophys. Res. Oceans 11949–11958.

Bylhouwer, B., Ianson, D., Kohfeld, K., 2013. Changes in the onset and intensity of wind-driven upwelling and downwelling along the North American Pacific coast. J. Geophys. Res. Oceans 118, 2565–2580. http://dx.doi.org/10.1002/jgrc.20194.

Cai, W.-J., Hu, X., Huang, W.-J., Murrell, M.C., Lehrter, J.C., Lohrenz, S.E., Chou, W.-C., Zhai, W., Hollibaugh, J.T., Wang, Y., Zhao, P., Guo, X., Gundersen, K., Dai, M., Gong, G.-C., 2011. Acidification of subsurface coastal waters enhanced by eutrophication. Nat. Geosci. 4, 766–770. http://dx.doi.org/10.1038/ngeo1297.

Canadian Fisheries Act: Wastewater Systems Effluent Regulations. Ministry of Justice retrieved from. http://laws-lois.justice.gc.ca/PDF/SOR-2012-139.pdf.

Capital Regional District, 2014. Macaulay and Clover Point Wastewater and Marine Environment Program 2013 Annual Report. (Victoria, BC, Canada).

Capital Regional District, 2017. Core Area Wastewater Treatment Program. Accessed online at. https://www.crd.bc.ca/docs/default-source/Wastewater-Planning-2014/Project-Board/appendix1crdbusinesscasefinal.pdf?sfvrsn=f4952cca_0 (Victoria, BC, Canada).

Chandler, P., 1997. Summary of CRD Mooring Program. (Victoria BC).

Chapman, P.M., 2006. Science, politics and ideology-the Victoria (BC, Canada) sewage issue. Mar. Pollut. Bull. 52, 719–721. http://dx.doi.org/10.1016/j.marpolbul.2006.03.006.

Chapman, P.M., 2007. Determining when contamination is pollution - weight of evidence determinations for sediments and effluents. Environ. Int. 33, 492–501.

Chapman, P.M., Paine, M.D., Arthur, A.D., Taylor, L.a., 1996. A triad study of sediment quality associated with a major, relatively untreated marine sewage discharge. Mar. Pollut. Bull. 32, 47–64. http://dx.doi.org/10.1016/0025-326X(95)00108-Y.

Chu, J.W.F., Tunnicliffe, V., 2015. Oxygen limitations on marine animal distributions and the collapse of epibenthic community structure during shoaling hypoxia. Glob. Chang. Biol. 21, 2989–3004. http://dx.doi.org/10.1111/gcb.12898.

Crawford, W.R., Peña, M.A., 2013. Declining oxygen on the British Columbia continental shelf. Atmosphere-Ocean 51, 88–103. http://dx.doi.org/10.1080/07055900.2012.753028.

Crawford, W.R., Peña, M.A., 2016. Decadal trends in oxygen concentration in subsurface waters of the Northeast Pacific Ocean. Atmosphere-Ocean 54, 171–192. http://dx.doi.org/10.1080/07055900.2016.1158145.

Crawford, W.R., Thomson, R.E., 1991. Physical oceanography of the western Canadian continental shelf. Cont. Shelf Res. 11, 669–683. http://dx.doi.org/10.1016/0278-4343(91)90073-F.

Davenne, E., Masson, D., Canada, F. and O, 2001. Water Properties in the Straits of Georgia and Juan de Fuca. Institute of Ocean Sciences, Sidney, BC, Canada.

Diaz, R.J., 1992. Sediment Profile Imaging (SPI) Survey of the Macaulay and Clover Point Wastewater Outfalls Victoria BC. EVS Consultants, North Vancouver, BC, Canada.

Diaz, R.J., Rosenberg, R., 2008. Spreading dead zones and consequences for marine ecosystems. Science (80-.) 321, 926–929. http://dx.doi.org/10.1126/science.1156401.

Diaz, R.J., Rosenburg, R., 1995. Marine benthic hypoxia: a review of its ecological effects and the behavioural responses of benthic macrofauna. Oceanogr. Mar. Biol. 33, 245–303.

Dickson, A.G., Sabine, C.L., Christian, J.R., 2007. Guide to best practices for ocean CO2 measurements. North Pacific Marine Science Organization.

Dinn, P.M., Johannessen, S.C., Macdonald, R.W., Lowe, C.J., Whiticar, M.J., 2012a. Effect of receiving environment on the transport and fate of polybrominated diphenyl ethers near two submarine municipal outfalls. Environ. Toxicol. Chem. 31, 566–573. http://dx.doi.org/10.1002/etc.1735.

Dinn, P.M., Johannessen, S.C., Ross, P.S., MacDonald, R.W., Whiticar, M.J., Lowe, C.J., Van Roodselaar, A., 2012b. PBDE and PCB accumulation in benthos near marine wastewater outfalls: the role of sediment organic carbon. Environ. Pollut. 171, 241–248. http://dx.doi.org/10.1016/j.envpol.2012.07.023.

Emerson, S., Hedges, J.I., 2008. Chemical Oceanography and the Marine Carbon Cycle. Cambridge University Press, Cambridge, UK, pp. 118–127.

Feely, R.A., Alin, S.R., Newton, J., Sabine, C.L., Warner, M., Devol, A., Krembs, C., Maloy, C., 2010. The combined effects of ocean acidification, mixing, and respiration on pH and carbonate saturation in an urbanized estuary. Estuar. Coast. Shelf Sci. 88, 442–449. http://dx.doi.org/10.1016/j.ecss.2010.05.004.

Garcia, H.E., Gordon, L.I., 1992. Oxygen solubility in seawater: better fitting equations. Limnol. Oceanogr. 37, 1307–1312.

Garcia, H.E., Gordon, L.I., 1993. Erratum: oxygen solubility in seawater: better fitting equations. Limnol. Oceanogr. 38, 656.

Gilbert, D., Rabalais, N.N., Díaz, R.J., Zhang, J., 2010. Evidence for greater oxygen decline rates in the coastal ocean than in the open ocean. Biogeosciences 7, 2283–2296. http://dx.doi.org/10.5194/bg-7-2283-2010.

Gómez, A.G., Juanes, J.A., Ondiviela, B., Revilla, J.A., 2014. Assessment of susceptibility to pollution in littoral waters using the concept of recovery time. Mar. Pollut. Bull. 81, 140–148. http://dx.doi.org/10.1016/j.marpolbul.2014.02.004.

Haigh, R., Ianson, D., Holt, C.A., Neate, H.E., Edwards, A.M., 2015. Effects of ocean acidification on temperate coastal marine ecosystems and fisheries in the Northeast Pacific. PLoS One 10, e0117533. http://dx.doi.org/10.1371/journal.pone.0117533.

Herlinveaux, R.H., Tully, J.P., 1961. Some oceanographic features of Juan de Fuca Strait. Fish. Res. Board Can. 18, 1027–1071. http://dx.doi.org/10.1139/f61-065.

Hodgins, D.O., 2006. Technical Memorandum: Assessment of the Plume Trapping and Dilution at the Clover Point Outfall and the Macaulay Point Outfall. Seaconsult Marine Research, Salt Spring Island, BC, Canada.

Hofmann, A.F., Peltzer, E.T., Walz, P.M., Brewer, P.G., 2011. Hypoxia by degrees: establishing definitions for a changing ocean. Deep-Sea Res. I 58, 1212–1226. http://dx.doi.org/10.1016/j.dsr.2011.09.004.

Ianson, D., Allen, S., 2002. A two-dimensional nitrogen and carbon flux model in a coastal upwelling region. Glob. Biogeochem. Cycles 16. http://dx.doi.org/10.1029/2001GB001451.

Ianson, D., Allen, S.E., Harris, S.L., Orians, K.J., Varela, D.E., Wong, C.S., 2003. The inorganic carbon system in the coastal upwelling region west of Vancouver Island, Canada. Deep-Sea Res. I 50, 1023–1042. http://dx.doi.org/10.1016/S0967-0637(03)00114-6.

Ianson, D., Allen, S.E., Moore-Maley, B.L., Johannessen, S.C., Macdonald, R.W., 2016. Vulnerability of a semi-enclosed estuarine sea to ocean acidification in contrast with hypoxia. Geophys. Res. Lett. http://dx.doi.org/10.1002/2016GL068996.

Igbinosa, E.O., Okoh, A.I., 2009. Impact of discharge wastewater effluents on the physico-chemical qualities of a receiving watershed in a typical rural community. Int. J. Environ. Sci. Technol. 6, 175–182.

Johannessen, S.C., Macdonald, R.W., 2009. Effects of local and global change on an inland sea: the Strait of Georgia, British Columbia, Canada. Clim. Res. 40, 1–21. http://dx.doi.org/10.3354/cr00819.

Johannessen, S.C., Masson, D., Macdonald, R.W., 2014. Oxygen in the deep Strait of Georgia, 1951–2009: the roles of mixing, deep-water renewal, and remineralization of organic carbon. Limnol. Oceanogr. 59, 211–222. http://dx.doi.org/10.4319/lo.2014.59.1.0211.

Johannessen, S.C., Macdonald, R.W., Burd, B., van Roodselaar, A., Bertold, S., 2015. Local environmental conditions determine the footprint of municipal effluent in coastal waters: a case study in the Strait of Georgia, British Columbia. Sci. Total Environ. 508, 228–239. http://dx.doi.org/10.1016/j.scitotenv.2014.11.096.

Krepakevich, A., Pospelova, V., 2010. Tracing the influence of sewage discharge on coastal bays of Southern Vancouver Island (BC, Canada) using sedimentary records of phytoplankton. Cont. Shelf Res. 30, 1924–1940. http://dx.doi.org/10.1016/j.csr.2010.09.002.

Krogh, Jeremy, 2017. Dissolved Oxygen and Inorganic Carbon Dynamics in a High-energy Coastal Environment. University of Victoria, Victoria, BC, Canada. http://hdl.handle.net/1828/8023.

Krogh, J., Lyons, S., Lowe, C.J., 2017. Pharmaceuticals and personal care products in municipal wastewater and the marine receiving environment near Victoria Canada. Front. Mar. Sci. 4, 415. http://dx.doi.org/10.3389/fmars.2017.00415.

Law, A.W.K., Tang, C., 2016. Industrial water treatment and industrial marine outfalls: achieving the right balance. Front. Chem. Sci. Eng. 10, 472–479. http://dx.doi.org/10.1007/s11705-016-1592-0.

LeBlond, P.H., 1983. The Strait of Georgia: functional anatomy of a coastal sea. Can. J. Fish. Aquat. Sci. 40, 1033–1063. http://dx.doi.org/10.1139/f83-128.

Li, S., Hodgins, D.O., 2004. A dynamically coupled outfall plume-circulation model for effluent dispersion in Burrard Inlet, British Columbia. J. Environ. Eng. Sci. 3, 433–449. http://dx.doi.org/10.1139/s04-039.

Li, S., Hodgins, D.O., 2010. Modelling wastewater effluent mixing and dispersion in a tidal channel. Can. J. Civ. Eng. 37, 99–111. http://dx.doi.org/10.1139/L09-128.

Lorax, 2009. Technical Memorandum, Backcasting Analysis of the Macaulay Point and Clover Point Outfalls During Times of High Observed Fecal Coliform Concentrations. Lorax Environmental Services Ltd., Vancouver, BC, Canada.

Lorax, 2012. Technical Memorandum, Baseline Outfall Assessment – Pre-treatment Conditions (2011). Lorax Environmental Services Ltd, Vancouver, BC, Canada.

Mackas, D.L., Harrison, P.J., 1997. Nitrogenous nutrient sources and sinks in the Juan de Fuca Strait/Strait of Georgia/Puget Sound estuarine system: assessing the potential for eutrophication. Estuar. Coast. Shelf Sci. 44, 1–21. http://dx.doi.org/10.1006/ecss.1996.0110.

Markovic, D.L., 2003. Untreated Municipal Sewage Discharge in Victoria Bight, British Columbia, Canada: An Investigation of Sediment Metal Contamination and Implications for Sustainable Development. Royal Roads University, Victoria, BC, Canada.

Masson, D., 2006. Seasonal water mass analysis for the straits of Juan de Fuca and Georgia. Atmosphere-Ocean 44, 1–15. http://dx.doi.org/10.3137/ao.440101.

McDougall, T.J., Barker, P.M., 2011. Getting Started With TEOS-10 and the Gibbs Seawater (GSW) Oceanographic Toolbox. SCOR/IAPSO WG127 (28 pp., ISBN 978-0-646-55621-5).

Moore-Maley, B.L., Allen, S.E., Ianson, D., 2016. Locally driven interannual variability of near-surface pH and Ω_A in the Strait of Georgia. J. Geophys. Res. Oceans 1600–1625. http://dx.doi.org/10.1002/2015JC011118.

Morrison, J., Quick, M.C., Foreman, M.G.G., 2002. Climate change in the Fraser River watershed: flow and temperature projections. J. Hydrol. 263, 230–244. http://dx.doi.org/10.1016/S0022-1694(02)00065-3.

Mote, P.W., Salathé, E.P., 2010. Future climate in the Pacific Northwest. Clim. Chang. 102, 29–50. http://dx.doi.org/10.1007/s10584-010-9848-z.

Parker, J.G., Rosell, R.S., MacOscar, K.C., 1988. The phytoplankton production cycle in Belfast Lough. J. Mar. Biol. Assoc. U. K. 68, 555–564. http://dx.doi.org/10.1017/S0025315400028708.

Pawlowicz, R., 2001. A tracer method for determining transport in two-layer systems, applied to the Strait of Georgia/Haro Strait/Juan de Fuca Strait estuarine system. Estuar. Coast. Shelf Sci. 52, 491–503. http://dx.doi.org/10.1006/ecss.2000.0748.

Pawlowicz, R., Riche, O., Halverson, M., 2007. The circulation and residence time of the strait of Georgia using a simple mixing-box approach. Atmosphere-Ocean 45, 173–193. http://dx.doi.org/10.3137/ao.450401.

Pearson, T., Rosenberg, Rutger, 1977. Macrobenthic succession in relation to organic enrichment and pollution of the marine environment. Oceanogr. Mar. Biol. Annu. Rev. 16, 229–311.

Philip, N.A., Pritchard, T.R., 1997. Australia's first deepwater sewage outfalls: design considerations and environmental performance monitoring. Mar. Pollut. Bull. 33, 140–146. http://dx.doi.org/10.1016/S0025-326X(96)00165-8.

Puente, A., Diaz, R.J., 2015. Response of benthos to ocean outfall discharges: does a general pattern exist? Mar. Pollut. Bull. 101, 174–181. http://dx.doi.org/10.1016/j.marpolbul.2015.11.002.

Rabalais, N.N., Díaz, R.J., Levin, L.A., Turner, R.E., Gilbert, D., Zhang, J., 2010. Dynamics and distribution of natural and human-caused hypoxia. Biogeosciences 7, 585–619. http://dx.doi.org/10.5194/bg-7-585-2010.

Ringuette, Janis, 2009. City of Gardens Was Once a City of Garbage. Accessed online at. http://www.beaconhillparkhistory.org/articles/122_garbage.htm.

Ronnberg, C., Bonsdorff, E., 2004. Baltic Sea eutrophication: area-specific ecological consequences. Hydrobiologia 514, 227–241. http://dx.doi.org/10.1023/B:HYDR.0000019238.84989.7f.

Schindler, D.W., Hecky, R.E., McCullough, G.K., 2012. The rapid eutrophication of Lake Winnipeg: greening under global change. J. Great Lakes Res. 38, 6–13. http://dx.doi.org/10.1016/j.jglr.2012.04.003.

Shampine, L.F., Reichelt, M.W., 1997. The MATLAB ODE suite. SIAM J. Sci. Comput. 18, 1–22.

Smith, V.H., Schindler, D.W., 2009. Eutrophication science: where do we go from here? Trends Ecol. Evol. 24, 201–207. http://dx.doi.org/10.1016/j.tree.2008.11.009.

Statistics Canada, 2012. Focus on Geography Series, 2011 Census. Statistics Canada

Catalogue No. 98-310-XWE2011004. Ottawa, Ontario. Analytical Products, 2011 Census. (Last updated October 24, 2012).
Tchobanoglous, G., Burton, F.L., 1991. Wastewater Engineering: Treatment, Disposal, and Reuse. McGraw-Hill.
Thomson, R.E., Mihály, S.F., Kulikov, E.a., 2007. Estuarine versus transient flow regimes in Juan de Fuca Strait. J. Geophys. Res. Oceans 112. http://dx.doi.org/10.1029/2006JC003925.
van Heuven, S., Pierrot, D., Rae, J.W.B., Lewis, E., Wallace, D.W.R., 2011. MATLAB Program Developed for CO_2 System Calculations. ORNL/CDIAC-105b. Carbon Dioxide Information Analysis Center, Oak Ridge National Laboratory, U.S. Department of Energy, Oak Ridge, Tennessee. http://dx.doi.org/10.3334/CDIAC/otg.CO2SYS_MATLAB_v1.1.
Welch, P.D., 1967. The use of fast Fourier transform for the estimation of power spectra: a method based on time averaging over short, modified periodograms. IEEE Trans. Audio Electroacoust. AU-15 (2), 70–73. http://dx.doi.org/10.1109/TAU.1967.1161901.